

Atomic resolution data reveal flexibility in the structure of RNase Sa

Jozef Ševčík,^{a*} Victor S. Lamzin,^b Zbigniew Dauter^c and Keith S. Wilson^d^aInstitute of Molecular Biology, Slovak Academy of Sciences, Bratislava, Slovak Republic,^bEuropean Molecular Biology Laboratory, Hamburg Outstation, Notkestrasse 85, 22603 Hamburg, Germany, ^cSynchrotron Radiation Research Section, Macromolecular Crystallography Laboratory, NCI, Brookhaven National Laboratory, Building 757A-X9, Upton, NY 11973, USA, and ^dStructural Biology Laboratory, University of York, York YO10 5DD, EnglandCorrespondence e-mail:
umbisevc@savba.savba.sk

Ribonuclease from *Streptomyces aureofaciens*, the bacterial source for the industrial production of chlorotetracycline, is a guanylate endoribonuclease (RNase Sa; EC 3.1.27.3) which hydrolyses the phosphodiester bonds of single-stranded RNA at the 3'-side of guanosine nucleotides with high specificity. The structure of the enzyme was previously refined at atomic resolution (1.2 Å) using room-temperature data. Here, the RNase Sa structure refined against 1.0 Å data collected at cryogenic temperature is reported. There are two surface loops in molecule *A* and one in molecule *B* for which two main-chain conformations are modelled: these loops contain active-site residues. The separation for most of the corresponding main-chain atoms in the two conformations is about 0.8 Å, with a maximum of 2.5 Å. The two regions of dual conformation represent the most important differences in comparison with the structure determined at room temperature, where the corresponding loops have one conformation only but the largest degree of anisotropy. The flexibility of the loops observed in the structure of RNase Sa is directly linked to the need for the active site to interact productively with substrates and/or inhibitors.

Received 15 May 2002

Accepted 6 June 2002

PDB Reference: RNase Sa,
1lni, 1lnisf.

1. Introduction

The structure of RNase Sa and of its complexes with guanosine-3'-monophosphate (3'-GMP; Sevcik *et al.*, 1991), guanosine-2'-monophosphate (2'-GMP; Sevcik, Hill *et al.*, 1993) and guanosine-2',3'-cyclophosphorothioate (2',3'-GCPT; Sevcik, Zegers *et al.*, 1993) as well as of the complex with barstar, the protein inhibitor of barnase from *Bacillus amyloliquefaciens* (Ševčík *et al.*, 1998), have been determined at high resolution. The native enzyme crystallizes in the orthorhombic space group $P2_12_12_1$, with unit-cell parameters $a = 39.0$, $b = 64.7$, $c = 78.6$ Å. There are two protein molecules in the asymmetric unit, which we hereafter refer to as molecules *A* and *B*. The structures of the apo enzyme (rt structure) and its complex with 2'-GMP were subsequently refined with anisotropic atomic displacement parameters (ADPs) using synchrotron data to 1.2 Å resolution recorded at room temperature (Sevcik *et al.*, 1996). Refinement converged with an *R* factor of 10.6% for the native structure and 10.9% for the complex with 2'-GMP. The overall r.m.s. coordinate error of the apo-enzyme structure as obtained from inversion of the normal matrix was 0.05 Å for all atoms (including 332 water molecules) and about 0.02 Å for main-chain atoms. The average ADPs for the protein in molecules *A* and *B* were 15.8 and 17.7 Å², respectively.

Here, we report the refinement of the structure of recombinant RNase Sa against 1.0 Å resolution synchrotron data collected at cryogenic temperature, 100 K (ct structure). The

structure shows a new feature which was not observed in the rt structures of RNase Sa; namely, two distinct conformations of the main-chain in two loops which contain active-site residues. The high mobility of the two conformations at room temperature presumably prevent them being resolved even with 1.2 Å resolution data: at 100 K the mobility is reduced and the 1.0 Å resolution data allow the two independent conformations to be distinguished.

The advantages of structures refined at atomic resolution have been reviewed in several papers (Dauter *et al.*, 1995, 1997, 2001; Longhi *et al.*, 1998). An important role in data-collection procedures is ascribed to flash-freezing techniques, which are routinely used in most laboratories. However, one has to realise that the structure at low temperature is not necessarily equivalent to that which functions under physiological conditions (Walsh *et al.*, 1998).

The accuracy of atomic resolution structures presents considerable advantages over those at lower resolution where restraints need to be used. Assumptions concerning the planarity of peptide groups have proved not to have absolute validity; significant discrepancies from planarity were observed in structures determined at atomic resolution (EU 3-D Validation Network, 1998), comparable to those seen in small-molecule peptide structures (MacArthur & Thornton, 1996). Similarly, the Ramachandran plot requires a slight revision. The accuracy of protein structures achieved at atomic resolution is important in some biological applications. Berisio *et al.* (1999) observed a strong correlation between the precise positions of several histidines and their ionization state in a series of atomic structures of RNase A at various pH values. Kachalova *et al.* (1999) have shown that binding of carbon monoxide to myoglobin at ambient temperatures requires concerted motion of the haem group, the Fe atom and two helices. The atomic resolution structure of LADH (Meijers *et al.*, 2001) identified the non-planarity of the cofactor NADH and an additional ligand site at the catalytic Zn atom and allowed the proposal of a modification of the classic catalytic mechanism of this enzyme.

2. Crystallization, data collection and processing

Recombinant RNase Sa was isolated and purified according to the procedure described by Hebert *et al.* (1997). The main steps were extraction of RNase Sa from the periplasmic space by osmotic shock, ion-exchange chromatography using an SP Sephadex C-25 column and gel-filtration chromatography on a Sephadex G-50 column. Yields of the protein from 1 l of media were up to 100 mg.

The recombinant enzyme was crystallized according to the same protocol as that used for crystallization of the enzyme isolated from the culture medium of *Streptomyces aureofaciens* (Sevcik *et al.*, 1991). In brief, crystals were grown by hanging-drop vapour diffusion from 1% protein solution in 0.1 M phosphate buffer pH 7.2. 25% saturated ammonium sulfate solution was used as precipitant. Immediately prior to freezing, the crystal was immersed for a few seconds in mother liquor containing in addition 25% of glycerol. The crystals

Table 1

Data collection and processing.

The data for the rt structure are taken from Sevcik *et al.* (1996).

	rt	ct
Data-collection temperature (K)	293	100
Beamline	X11	X11
Space group	$P2_12_12_1$	$P2_12_12_1$
Unit-cell parameters (Å)		
<i>a</i>	39.05	38.28
<i>b</i>	64.82	64.20
<i>c</i>	78.56	77.80
Wavelength (Å)	0.920	0.934
Maximum resolution (Å)	1.2	1.0
Unique reflections	60670	101172
Overall completeness (%)	95.3	97.5
$R(I)_{\text{merge}}^\dagger$ (%)	3.9	4.2
$I/\sigma(I)$	18.5	28.7
Outer resolution range (Å)	1.25–1.2	1.02–1.0
Completeness (%)	91.0	91.1
$R(I)_{\text{merge}}$ (%)	17.0	53.9
$I/\sigma(I)$	—	2.4

$^\dagger R(I)_{\text{merge}} = \sum |I - \langle I \rangle| / \sum I$, where I is an individual intensity measurement and $\langle I \rangle$ is the average intensity for this reflection with summation over all data.

belonged to the orthorhombic space group $P2_12_12_1$, with unit-cell parameters $a = 38.28$, $b = 64.20$, $c = 77.80$ Å and two protein molecules in the asymmetric unit. The size of the crystal used to collect diffraction data was about $0.4 \times 0.5 \times 0.25$ mm.

X-ray data were collected at low temperature, 100 K, on the EMBL beamline X11 at the DORIS storage ring, DESY, Hamburg, Germany with a MAR Research (Hamburg) imaging-plate scanner. To avoid the loss of the strongest reflections owing to saturation, three sets of data to 1.0, 1.8 and 2.5 Å resolution were collected with exposures differing by approximately tenfold between the successive sets. The data were processed with *DENZO* (Otwinowski & Minor, 1997). A summary of data collection and processing is given in Table 1. For comparison purposes, the values for the rt structure (Sevcik *et al.*, 1996) are also given. The ratio of measured reflections to refined positional and anisotropic thermal parameters is 6.0 (compared with 3.5 at 1.2 Å resolution). This allowed refinement of at least the best ordered part of the structure without any restraints.

3. Refinement of the structure

For structure refinement, a protocol was used similar to that for the rt structure at 1.2 Å (Sevcik *et al.*, 1996). The starting model for the refinement was the RNase Sa coordinate set 1rgg (1.2 Å RNase Sa) from the Protein Data Bank (Berman *et al.*, 2000), from which all double conformations and solvent molecules were excluded. Positions of all atoms were randomized with an r.m.s. displacement of 0.3 Å. The first 30 cycles of refinement were carried out with the *CCP4* (Collaborative Computational Project, Number 4, 1994) version of the program *PROLSQ* (Konnert & Hendrickson, 1980), resulting in a drop in the R factor from 49 to 21%. At this stage, H atoms were included at their idealized positions that

were recalculated after each refinement cycle. A further 15 cycles of refinement with *PROLSQ* lowered the *R* factor to 19.8%. The next 15 cycles of refinement were performed with *SHELXL93* (Sheldrick, 1993) with isotropic temperature factors. In all subsequent steps, *SHELXL* with anisotropic temperature factors was used. To obtain estimates of individual errors of the refined parameters, a round of block-matrix refinement was performed as a final step. Each block consisted of 30 residues and the blocks overlapped by one residue. Coordinate errors for main-chain atoms estimated from matrix inversion are shown in Fig. 1.

After each refinement step, *ARP* (Lamzin & Wilson, 1997) was used for modelling and updating the solvent structure. When the *R* factor had fallen to about 13%, the electron density became clear enough to allow two conformations of the main chain to be evident in two regions of the structure. Two main-chain conformations were built for two surface loops in molecule *A* (residues 25–42 and 82–86), but only for one in molecule *B* (23–27). In addition, alternative conformations were modelled for the side chains of Arg65, Glu74, Thr76 and Leu91 in molecule *A* and Thr5, Gln38, Ile58, Thr76 and Ser90 in molecule *B*. Refinement of two protein molecules, one sulfate anion, three glycerol molecules and 557 water molecules in the asymmetric unit converged with *R* = 11.9% for all 101 172 unique reflections (Table 2). For comparison purposes, the values for the *rt* structure (Sevcik *et al.*

Table 2

Refinement statistics.

The data for the *rt* structure are taken from Sevcik *et al.* (1996).

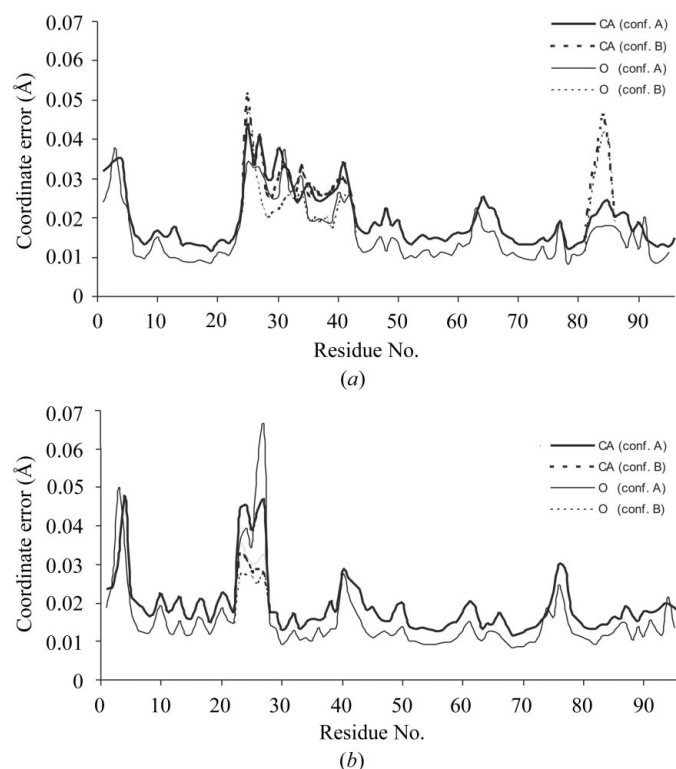
	<i>rt</i>	<i>ct</i>
Resolution limits (Å)	10.0–1.2	19.5–1.0
<i>R</i> factor (%)	10.6	11.9
Water molecules	332	557
SO ₄ ²⁻ ions	1	1
Glycerol molecules	—	3
Wilson plot <i>B</i> factor (Å ²)	10.8	7.1
Average <i>B</i> (Å ²)		
Main chain		
Molecule <i>A</i>	13.4	8.6
Molecule <i>B</i>	15.3	8.9
Side chain		
Molecule <i>A</i>	18.2	9.5
Molecule <i>B</i>	20.2	12.0
Waters	42.0	34.0
Ions	16.4	8.1
Glycerol	—	18.3

al., 1996) are also presented. The occupancies of dual conformations were refined individually with the sum of the occupancies of corresponding atoms being set to unity. Occupancies of water molecules (except W1–W7, which belong to one of the dual protein conformations) were not refined but were set to unity. The program *O* (Jones, 1978) was used for visualizing and rebuilding purposes.

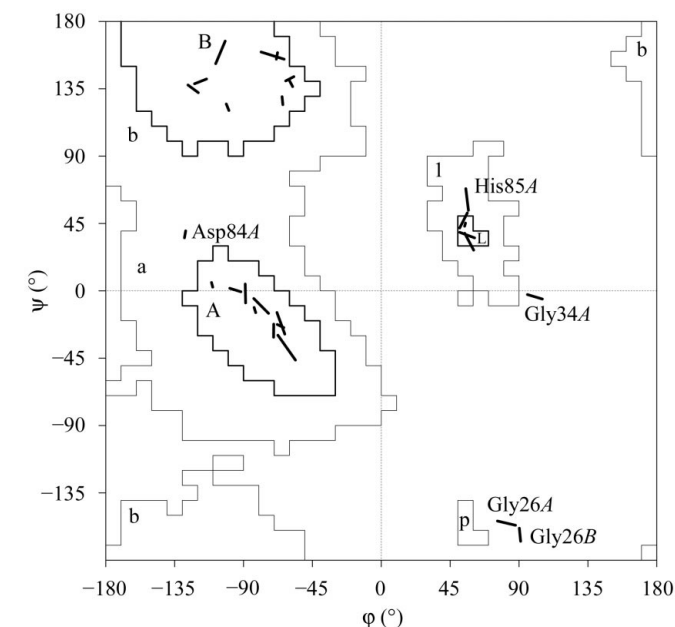
4. Discussion

4.1. Accuracy of the model

The Ramachandran plot (Ramakrishnan & Ramachandran, 1965) calculated by the program *PROCHECK* (Laskowski *et al.*, 1993) shows that 91.2% of the residues are in most

**Figure 1**

Coordinate errors for main-chain CA and O atoms estimated from matrix inversion for (a) molecule *A* and (b) molecule *B*. Error estimates for the second conformation are presented as dashed lines. For the purpose of clarity, the errors for N and C atoms are not shown; they generally lie between those outlined for CA and O atoms.

**Figure 2**

Difference Ramachandran plot for residues in segments with two conformations. The end points of lines represent θ and ψ angles.

favoured regions and the rest are in additionally allowed regions. The Ramachandran plot for the segments with two main-chain conformations was performed separately (Fig. 2). The end points of the thick lines show the 'difference' Ramachandran plot (Kleywegt, 1996).

The overlap of *A* and *B* molecules from the rt and ct structures using least-squares minimization of distances between corresponding CA atoms is given in Table 3. For overlap, only CA atoms with single conformation were used. The overlap shows that flash-freezing did not cause significant conformational changes except for atoms in the loops with two main-chain conformations.

4.2. Temperature factors

The average temperature factors for main chain, side chain, water molecules, ions and glycerol molecules for rt and ct structures are given in Table 2. The bar diagram in Fig. 3 shows the average temperature factors for main-chain atoms as a function of residue number for ct and rt structures. While the *B* values are lower in the ct structure, they show a similar pattern of variation at the two temperatures. The overall mean anisotropy for molecules *A* and *B* of the ct structure is 2.07 and 1.92, respectively. The values are similar for both molecules and could be taken to imply that the anisotropic characteristics of RNase Sa are an intrinsic property of the molecule itself and do not depend much on the packing in the crystal. However, the anisotropy was only computed for 445 atoms in molecule *A* and 702 in *B*, as the atoms belonging to the loops with two conformations were refined with isotropic models, somewhat reducing the significance of this conclusion. For comparison, the overall mean anisotropy for molecule *A* and *B* of the rt structure computed for all atoms is 1.68 and 1.64, respectively.

4.3. Comparison of the room-temperature and low-temperature structures

In general, the ct structure is very similar to the rt structure described previously (Sevcik *et al.*, 1996); therefore, the following discussion is focused on the features which are different. In brief, the structure of RNase Sa consists of one α -helix and adjacent to it a three-stranded anti-parallel β -sheet which contains residues forming the catalytic site.

The electron density in the ct structure is very clear, as expected for structures at atomic resolution. The quality of the electron density even in the early stages of the refinement allowed the identification of two conformations of the main chain and corresponding side

chains for two regions in molecule *A*, residues 25–42 and 82–86, and one region in molecule *B*, residues 23–27. Fig. 4 shows the electron density for a short segment of loop 25–42 in molecule *A* of the ct structure, where the separation between

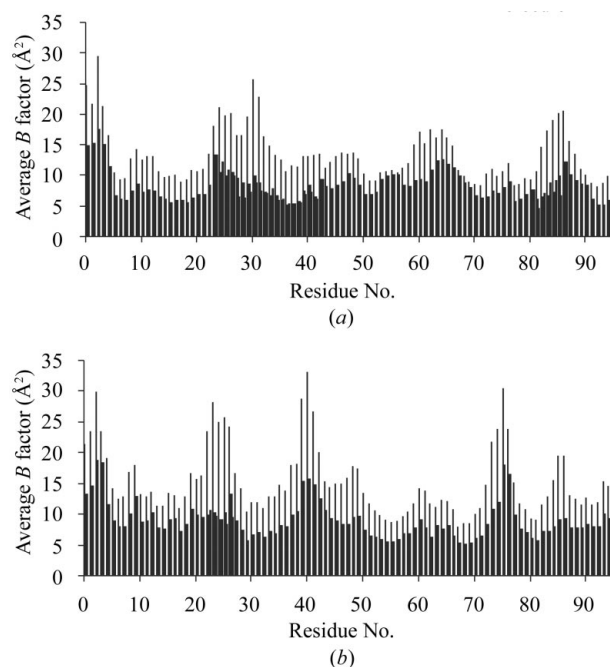


Figure 3 Average temperature factors from rt (light lines) and ct (heavy lines) structures for main chain of (a) molecule *A* and (b) molecule *B*. Regions with two main-chain conformations are clearly seen.

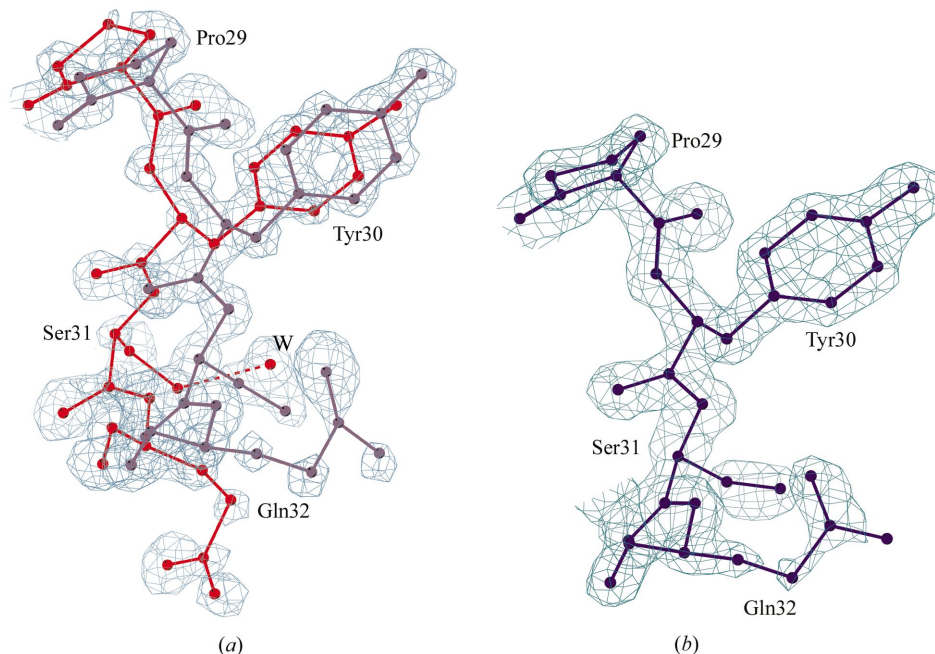


Figure 4 (a) $(3F_o - 2F_c, \alpha_c)$ electron density contoured at 1.0σ showing two conformations of the Pro29–Gln32 segment in molecule *A* of the ct structure. (b) The same segment of the rt structure with electron density contoured at 2σ . These figures were produced using *BobScript* (Esnouf, 1997).

Table 3
Overlap of CA atoms of *A* and *B* molecules in rt and ct structures.

rt	ct	R.m.s. dev. (Å)	Max. dev. (Å)	Position of max. deviation
<i>A</i>	<i>A</i>	0.21	0.45	Arg65, Asp1
<i>B</i>	<i>B</i>	0.17	0.44	Thr64, Gly4
<i>A–B</i>		0.38	1.46	Arg63
	<i>A–B</i>	0.50	1.80	Arg63

the main-chain atoms is largest. For comparison, the same region of the rt structure is also shown. The occupancies of all atoms belonging to one of the two conformations of the three stretches are the same: 0.49 and 0.51 (*A25–A42*), 0.37 and 0.63 (*A82–A86*), and 0.40 and 0.60 (*B23–B27*).

The segments in double conformations are a part of surface loops and contain catalytic and binding-site residues. The reason why in the *B* molecule two conformations of main-chain are seen only at the beginning of the longer loop (residues 23–27) can be attributed to the different crystal packing environment of the two molecules. In molecule *A*, Pro29 and Tyr30 belonging to the two conformations of the loop 25–42 form two relatively short non-bonded contacts with Thr46 of the neighbouring molecule *B*. Pro29 and Tyr30 slide around Thr46. It seems that the extent of this movement is limited by a 3.18 Å contact between Thr46 CG2 and the Pro29 main-chain O atom belonging to one conformation and a 3.27 Å contact between Thr46 CB and Tyr30 OH of the other conformation (Fig. 5*a*). In molecule *B*, Tyr30 OH and the main-chain N atom of Ser31 make 2.56 and 2.94 Å hydrogen bonds with molecule *A* Gln77 NE2 and Gln94 main-chain O atom, respectively (Fig. 5*b*), which make it impossible for the loop to move.

Different crystal packing is also responsible for different accessibility of the active sites of molecules *A* and *B*. While the active site of molecule *A* faces a large cavity in the crystal, the active site of molecule *B* is in close proximity to a neighbouring molecule, with His85 NE2 only 3.55 Å from the Asn20 main-chain O atom of molecule *A*. These differences in accessibility of the active sites of molecules *A* and *B* were also manifest in the structures of complexes with the mononucleotides 2'-GMP, 3'-GMP and 2',3'-GCPT obtained by soaking the native crystals in appropriate solutions. The nucleotides bound only to the active site of molecule *A*, with the exception of 2'-GMP, which was bound also to molecule *B* at low occupancy. The 3'-GMP and 2',3'-GCPT inhibitors could not enter the active site of molecule *B*, as their molecules are about 1 Å longer than 2'-GMP.

The overlap of the rt and ct structures shows that the loops with two main-chain conformations are evenly spread around the single conformation at rt except for a short segment in the vicinity of Ser31, for which the separation of CA atoms reaches 2.5 Å. The typical distance between corresponding main-chain atoms in the two conformations is 0.8 Å. These loops in the rt structure do not show clear evidence for two conformations. However, the anisotropic displacement of atoms in the room-temperature structure represented by

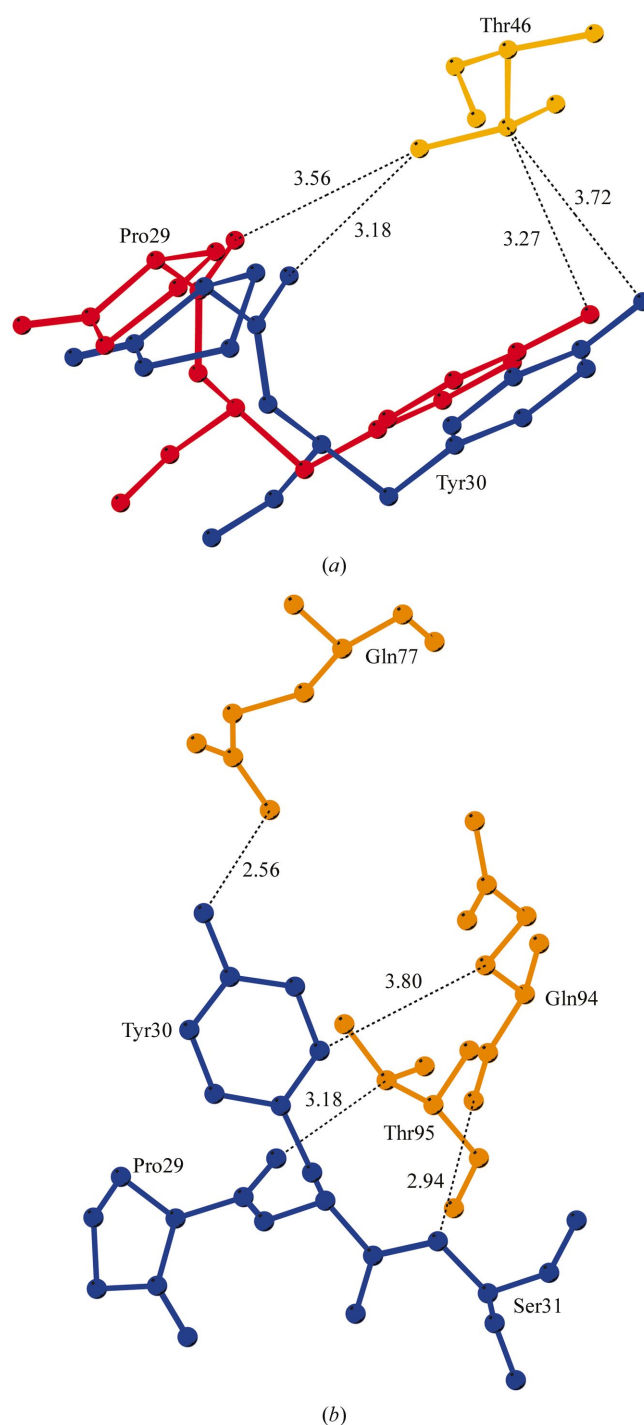


Figure 5

The influence of different crystal packing on the conformation of the 25–42 loop. Shortest contacts (Å) represented by dashed lines formed by molecules *A* and *B* with the neighbouring molecule are shown in (a) and (b), respectively. The two conformations are in blue and red; residues from the neighbouring molecule are in orange.

thermal ellipsoids (Fig. 6*b*) corresponds in direction and size to the positions of respective main-chain atoms in the two conformations of the ct structure (Fig. 6*a*). The overlap of the two structures also shows that water molecules at the active site which were identified previously (Sevcik *et al.*, 1991) are

also present in the ct structure. These water molecules are conserved in all RNase Sa structures with a free active site determined at room as well as at cryogenic temperature, as for example that of the T95A mutant of RNase Sa (Urbanikova, unpublished work).

Overlap of molecule *A* from the RNase Sa–3'-GMP complex structure (2sar) with molecule *A* from the ct structure based on least-squares superposition of 73 CA atoms which have only one conformation in ct gives an r.m.s. deviation of 0.24 Å and a maximum deviation of 0.53 Å at residue Arg63. Fig. 7 shows the loops with two conformations in molecule *A* of the ct structure with the mononucleotide modelled into the

active site. The movement of the loops which can be characterized as 'open' and 'closed' in respect to the 3'-GMP molecule is obvious. The conformation of the loops after binding the inhibitor to the active site is almost identical to the 'closed' conformation of the ct structure, *i.e.* the 'closed' conformation is that which the enzyme adopts after binding the substrate or inhibitor. The Arg40 side chain in the 'closed' conformation forms a stacking interaction with the base of the mononucleotide located between Arg40 and the bottom of the active site which is represented by Phe37 and Tyr86. The distances between the 3'-GMP base and the stacking partners

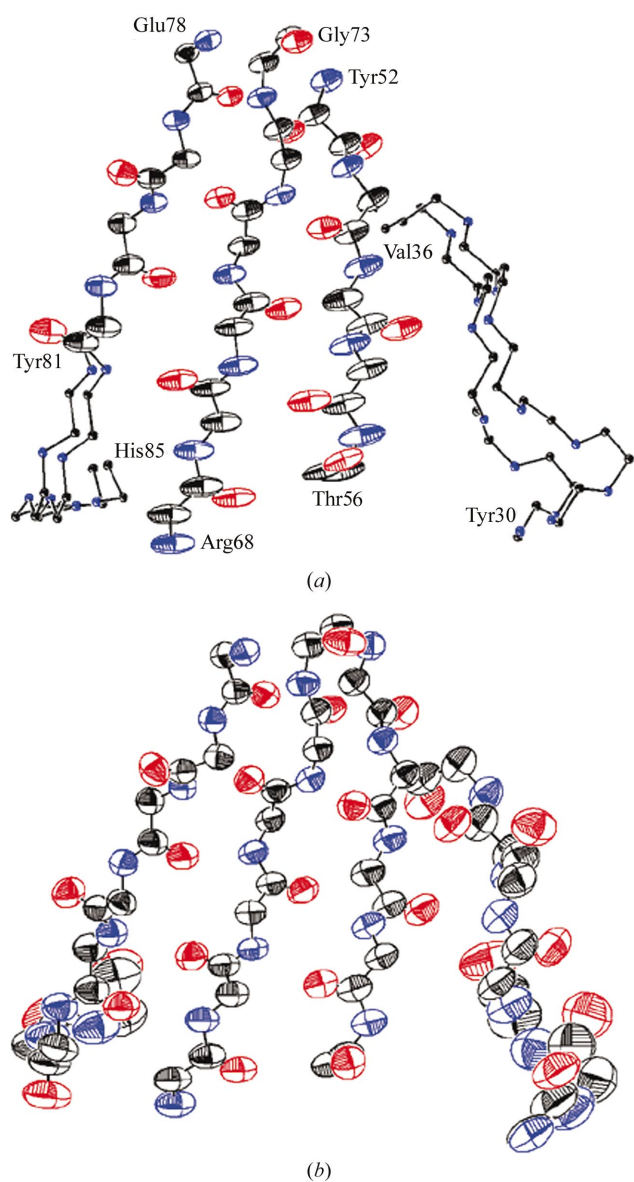


Figure 6
(a) Part of molecule *A* of the ct structure, showing two main-chain conformations (refined with isotropic thermal parameters). Thermal ellipsoids are shown for atoms refined anisotropically. (b) Respective part of the rt structure. The largest anisotropy is seen in parts which in the ct structure have two main-chain conformations. Ellipsoids were plotted using the program *ORTEP* (Burnett & Johnson, 1996).

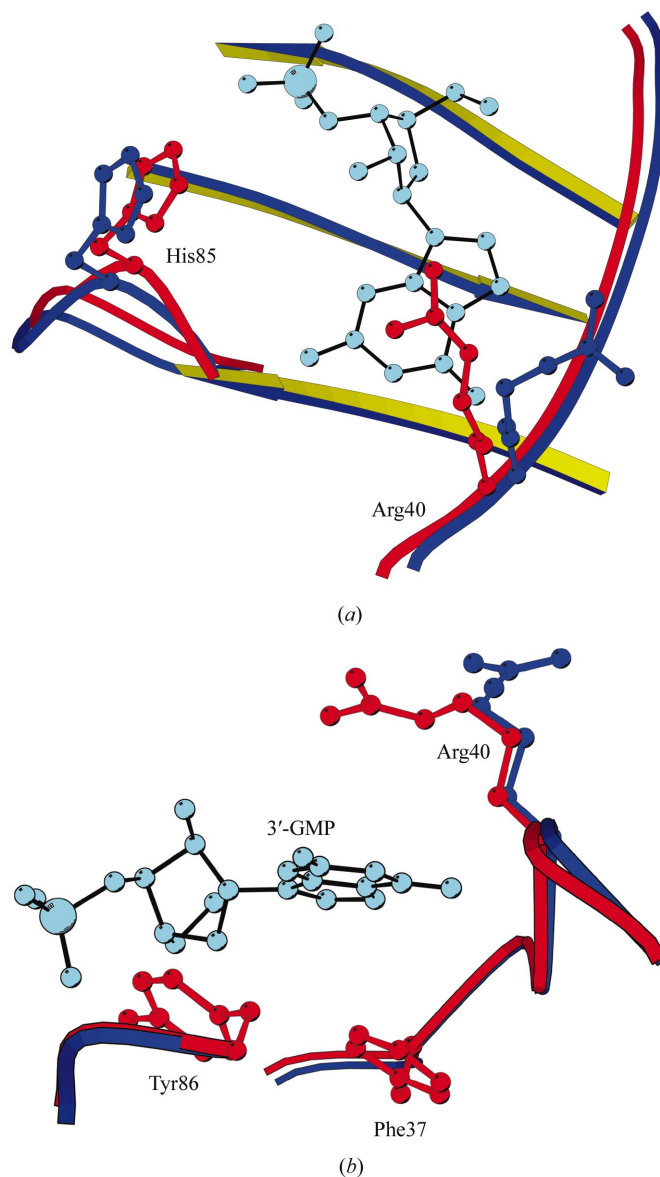


Figure 7
The 3'-GMP molecule modelled into the active site of molecule *A* of the ct structure. The loops, including the Arg40 side chain, are shown in the 'closed' (red) and 'open' (blue) conformations in views (a) perpendicular to the 3'-GMP base and (b) parallel to the base. The distances between the base and its stacking partners are 3.5 Å. His85 is the catalytic residue; Phe37 and Tyr86 are the residues forming the bottom of the active site. The figure was drawn using *MOLSCRIPT* (Kraulis, 1991).

are close to 3.5 Å. In the structures of the complexes of RNase Sa with mononucleotides, the 'closed' conformation of Arg40 was seen only in molecule *B* in the complex with 2'-GMP, the only complex in which the inhibitor was also bound to molecule *B* (Sevcik, Hill *et al.*, 1993). In molecules *A* of all RNase Sa structures with a free active site, Arg40 is in the open conformation in which it forms three hydrogen bonds: an intramolecular bond with Gln38 OE1 and two intermolecular lattice contacts with the main-chain O atoms of Gly61 and Glu74 of a neighbouring molecule. The Arg40 side chain becomes highly disordered in complex structures, presumably owing to its tendency to close the active site, which is hindered by the attractive forces caused by its hydrogen-bonding partners in the crystal.

Another example of RNase Sa flexibility is seen in the loop around Arg63. Overlap of molecules *A* and *B* shows differences in the main-chain atoms of up to 1.6 Å owing to a different crystal environment.

A sulfate anion was modelled at the site of Arg63 of molecule *A* (as in all RNase Sa structures refined so far). It forms a network of hydrogen bonds with Arg63 of molecule *A* and Arg68 of the neighbouring molecule *B*. This anion was not seen in molecule *B* owing to the different packing environment. The average distance between the central atom and four O atoms in the ion is 1.45 and 1.47 Å in ct and rt structures, respectively, which confirms that it is a sulfate anion (ideal S—O distance is 1.49 Å) and not phosphate (P—O distance is 1.56 Å). In the mother liquor, both sulfate (precipitant) and phosphate (buffer) are present.

5. Concluding remarks

The structure of RNase Sa determined at 1.0 Å resolution with data collected at cryogenic temperature (ct) suggests that there are two alternative conformations for residues in two loops close to the active site which lie in one of the most flexible parts of the structure. This is in contrast to what is observed in the rt structure (Sevcik *et al.*, 1996), where the slightly lower resolution and the higher overall mobility prevent the two conformations being resolved; instead, they are modelled by a single highly anisotropic conformation. The differences in the movement of the loops in molecules *A* and *B* show the effect of crystal contacts on the equilibrium between the two conformations. The extent of the movement is comparable to that observed in the structures of RNase Sa determined by NMR (Laurents *et al.*, 2001), *i.e.* it shows the flexibility of a part of the molecule, as can be seen in solution. The two conformations of the loops can be presumed to facilitate the structural adaptation required for productive interactions with substrates and inhibitors. This is supported by the fact that the closed conformation is observed in the complexes with nucleotide.

This work was supported by Howard Hughes Medical Institute grant No. 75195-574601 and the Slovak Academy of Sciences grant No. 2/1010/96.

References

- Berisio, R., Lamzin, V. S., Sica, F., Wilson, K. S., Zagari, A. & Mazzarella, L. (1999). *J. Mol. Biol.* **292**, 845–854.
- Berman, H. M., Westbrook, J., Feng, Z., Gilliland, G., Bhat, T. N., Weissig, H., Shindyalov, I. N. & Bourne, P. E. (2000). *Nucleic Acids Res.* **28**, 235–242.
- Burnett, M. N. & Johnson, C. K. (1996). *ORTEP-III: Oak Ridge Thermal Ellipsoid Plot Program for Crystal Structure Illustrations*, Oak Ridge National Laboratory Report ORNL-6895.
- Collaborative Computational Project, Number 4 (1994). *Acta Cryst.* **D50**, 760–763.
- Dauter, Z., Lamzin, V. S. & Wilson, K. S. (1995). *Curr. Opin. Struct. Biol.* **5**, 784–790.
- Dauter, Z., Lamzin, V. S. & Wilson, K. S. (1997). *Curr. Opin. Struct. Biol.* **7**, 681–668.
- Dauter, Z., Murshudov, G. N. & Wilson, K. S. (2001). *International Tables for Crystallography*, Vol. F, edited by M. G. Rossmann & E. Arnold, ch. 18.4. Dordrecht: Kluwer Academic Publishers.
- Esnouf, R. M. (1997). *J. Mol. Graph.* **15**, 132–134.
- EU 3-D Validation Network (1998). *J. Mol. Biol.* **276**, 417–436.
- Hebert, E. J., Grimsley, G. R., Hartley, R. W., Horn, G., Schell, D., Garcia, S., Both, V., Sevcik, J. & Pace, C. N. (1997). *Protein Expr. Purif.* **11**, 162–168.
- Jones, T. A. (1978). *J. Appl. Cryst.* **11**, 268–272.
- Kachalova, G. S., Popov, A. N. & Bartunik, H. D. (1999). *Science*, **284**, 473–476.
- Kleywegt, G. J. (1996). *Acta Cryst.* **D52**, 842–857.
- Konnert, J. H. & Hendrickson, W. A. (1980). *Acta Cryst.* **A36**, 344–350.
- Kraulis, P. J. (1991). *J. Appl. Cryst.* **24**, 946–950.
- Lamzin, V. S. & Wilson, K. S. (1997). *Methods Enzymol.* **277**, 269–305.
- Laskowski, R. A., MacArthur, M. W., Moss, D. S. & Thornton, J. M. (1993). *J. Appl. Cryst.* **26**, 283–291.
- Laurents, D. L., Perez-Canadillas, J. M., Santoro, J., Rico, M., Schell, D., Pace, C. N. & Bruix, M. (2001). *Proteins Struct. Funct. Genet.* **44**, 200–211.
- Longhi, S., Czjzek, M. & Cambillau, C. (1998). *Curr. Opin. Struct. Biol.* **8**, 730–737.
- MacArthur, M. W. & Thornton, J. M. (1996). *Protein Eng.* **8**, 217–224.
- Meijers, R., Morris, R. J., Adolph, H. W., Merli, A., Lamzin, V. S. & Cedergren-Zeppezauer, E. S. (2001). *J. Biol. Chem.* **276**, 9316–9321.
- Otwinowski, Z. & Minor, W. (1997). *Methods Enzymol.* **276**, 307–326.
- Ramakrishnan, C. & Ramachandran, G. N. (1965). *Biophys. J.* **5**, 909–933.
- Sevcik, J., Dauter, Z., Lamzin, V. S. & Wilson, K. S. (1996). *Acta Cryst.* **D52**, 327–344.
- Sevcik, J., Dodson, E. J. & Dodson, G. G. (1991). *Acta Cryst.* **B47**, 240–253.
- Sevcik, J., Hill, C., Dauter, Z. & Wilson, K. S. (1993). *Acta Cryst.* **D49**, 257–271.
- Ševčík, J., Urbanikova, L., Dauter, Z. & Wilson, K. S. (1998). *Acta Cryst.* **D54**, 954–963.
- Sevcik, J., Zegers, I., Wyns, L., Dauter, Z. & Wilson, K. S. (1993). *Eur. J. Biochem.* **216**, 301–305.
- Sheldrick, G. M. (1993). *SHELXL93 Program For Crystal Structure Refinement*. University of Göttingen, Germany.
- Walsh, M. A., Schneider, T. R., Sieker, L. C., Dauter, Z., Lamzin, V. S. & Wilson, K. S. (1998). *Acta Cryst.* **D54**, 522–526.